ELSEVIER

Polymer 42 (2001) 7349–7362

polymer

www.elsevier.nl/locate/polymer

Hydrophobic recovery of polydimethylsiloxane after exposure to partial discharges as a function of crosslink density

H. Hillborg[a,b], M. Sandelin[a], U.W. Gedde[a,*]

[a]*Department of Polymer Technology, Royal Institute of Technology, SE-100 44 Stockholm, Sweden*
[b]*Department of High Voltage Engineering, ABB Corporate Research, SE-721 78 Västerås, Sweden*

Received 24 January 2001; received in revised form 12 March 2001; accepted 14 March 2001

Abstract

Polydimethylsiloxanes with different crosslink densities were exposed to corona discharges or GHz air plasma and studied by contact angle measurements, X-ray photoelectron spectroscopy, optical microscopy, scanning electron microscopy and atomic force microscopy. The degree of surface oxidation increased with increasing exposure time with a limiting depth of 100–150 nm. Surface oxidation was faster in more highly crosslinked polymers. Within the oxidised layer, a brittle, microporous silica-like layer with a minimum organic silicone content of 40% gradually developed with increasing exposure time. The strain at which the silica-like layer cracked decreased with increasing dose of corona or air plasma. The hydrophobic recovery following the corona/air plasma exposure occurred at a slow rate by diffusion of oligomers through the microporous but uncracked silica-like layer or at a much higher rate by transport of oligomers through cracks in the silica-like layer.

Keywords: Polydimethylsiloxane; Electrical discharges; Hydrophobicity

1. Introduction

Silicone rubber based on polydimethylsiloxane (PDMS) is replacing porcelain and glass in high-voltage outdoor insulators due to its low density, vandalism resistance and water-repellent surface properties. Silicone rubber generally exhibits a better electrical performance during severe service conditions than glass and porcelain [1,2] and other rubber compounds, e.g. EPDM [3,4]. Similar observations have been made in laboratory tests [5,6]. The advantage of PDMS is its low surface energy — 16–21 mN m^{-1}, the precise value depending on the molar mass [7] — which means that it has a water-repellent surface that prevents extensive wetting of the insulation. This prevents leakage currents from developing across the surface. Under certain conditions, i.e. heavy rain, salt fog or severe pollution, electrical discharges may occur at the surface and lead to a loss of hydrophobicity. After a relatively short period of time with no discharge activity, typically ranging from a few hours to a few days, the hydrophobicity is regained. This is referred to as hydrophobic recovery. The hydrophobic recovery of PDMS has been attributed to a reorientation of methyl and hydroxyl groups by conformational changes [8,9], condensation of silanol groups [8] and the diffusion of low molar mass PDMS species to the surface [9–14]. The low molar mass PDMS species are degradation products formed at elevated temperatures [15–19] or during exposure to electrical discharges [9]. They may also be present in the rubber as residues from the polymerisation process or as added processing agents. The low molar mass PDMS embeds pollutants present on the surface on the silicone rubber surfaces and this enhances the surface hydrophobicity [3].

Electrical discharges by corona or air plasma initiate a range of chemical reactions in PDMS. Both chain scission and crosslinking occur, the latter leading to the formation of a silica-like surface layer [9,12–14,20–23]. The silica-like layer may under some conditions retard the hydrophobic recovery [13,14,21]. Fracture of the silica layer, caused by internal stresses or by external mechanical stresses, accelerates the hydrophobic recovery [13,14,21], suggesting that a surface-tension-driven migration of low molar mass species occurs through the surface cracks [12–14,22]. X-ray photoelectron spectroscopy (XPS) showed that the topmost layer in a specimen with recovered hydrophobicity was very similar to that of the unexposed material, whereas the layer beneath remained oxidised [9,14,20]. According to neutron reflectometry, the smooth oxidised surface layer was

* Corresponding author. Tel.: +46-8-7907640; fax: +46-8-208856.
E-mail address: gedde@polymer.kth.se (U.W. Gedde).

0032-3861/01/$ - see front matter
PII: S0032-3861(01)00202-6

130–160 nm thick [22]. The oxidised layer contained a mixture of the unoxidised polymer and silicon bonded to three or four oxygen atoms [22].

This paper presents data for a range of well-defined PDMS networks, differing only in crosslink density, exposed to a corona discharge or air plasma. The loss and recovery of hydrophobicity was assessed by contact angle measurements and was related to chemical and morphological changes of the surface as revealed by XPS, optical microscopy, atomic force microscopy (AFM) and scanning electron microscopy (SEM). Both corona and air plasma treatments led to a loss of hydrophobicity. The degree of surface oxidation increased with increasing dose and the rate of oxidation was higher in the densely crosslinked polymers. As a result, a vitrified, silica-like surface layer with low surface roughness gradually grew and finally approached the thickness of the oxidised layer. The thickness of the silica-like layer ranged between 10 and 100 nm. It was shown that the thickness and the fracture properties of the silica-like layer largely controlled the rate of hydrophobic recovery.

2. Experimental

2.1. Preparation of crosslinked polydimethylsiloxanes

Vinyldimethyl-terminated PDMSs were crosslinked in a hydrosilylation reaction, using a (30–35%) methylhydro-(65–70%) dimethylsiloxane copolymer with $\bar{M}_w = 2100\ g\ mol^{-1}$ as crosslinker. The ratio of hydride to vinyl groups was 2:1 in order to achieve fully a crosslinked network structure [24]. A platinum divinyltetramethyl disiloxane complex was used as a catalyst at a concentration of 30 ppm. The chemicals were purchased from United Chemical Technologies, USA, and were used as received. The molar mass distribution of the vinyldimethyl-terminated PDMS was assessed by size exclusion chromatography, using $CHCl_3$ as solvent. PDMS standards, purchased from Polymer Source, Canada, were used for calibration. Sheets of crosslinked PDMS with a thickness of 1 mm and a diameter of 210 mm were prepared in a Schwabenthan Polystat 400S compression moulding machine at 135°C and 6 MPa pressure for 15 min. Postcuring was performed in an oven at 120°C for 12 h. Specimens with a diameter of 30 mm were cut from the moulded sheets. Low molar mass species were removed from the specimen by Soxhlet extraction during 72 h, using hexane (boiling point = 68°C) as solvent. The specimens were slowly dried in air, further dried in a vacuum-oven and kept in desiccators. The number average molar mass of the chain segments between the crosslinks ($\bar{M}_c$) of the PDMS networks are assumed to be equal to number average molar mass ($\bar{M}_n$) of the particular vinyldimethyl-terminated PDMS used. The codes used for the different PDMS networks are as follows: P0.7, $\bar{M}_c = 700\ g\ mol^{-1}$; P8, $\bar{M}_c = 7500\ g\ mol^{-1}$; P12, $\bar{M}_c = 11\,600\ g\ mol^{-1}$; P17, $\bar{M}_c = 16\,500\ g\ mol^{-1}$; P38, $\bar{M}_c = 38\,300\ g\ mol^{-1}$. The polydispersity ($\bar{M}_w/\bar{M}_n$) of the vinyldimethyl-terminated PDMSs were 1.1 (P0.7), 1.5 (P8), 1.6 (P12), 1.9 (P17) and 1.5 (P38).

2.2. Density measurements

The densities of the PDMS materials were determined at 23°C in a density gradient column prepared from ethanol and water according to ASTM D1505-68. Four specimens of each material were used for the measurements.

2.3. Mechanical testing

An Instron 5566 equipped with a non-contact video extensiometer was used to determine the Young's modulus of the different materials. The measurements were performed according to ISO 1184-1983(E) at 22 ± 2°C and 40 ± 10% RH. Dumb-bell-shaped specimens were punched out from the films using a punch die (ISO 37, type 2). Six specimens of each material were tested.

2.4. Corona discharges

Specimens were subjected to corona discharges in dry air (<2% RH) at normal pressure using a set-up described by Hillborg and Gedde [14]. The applied 50 Hz AC voltage was 20 kV_{peak} between the 87 mm diameter electrode containing 31 needles and the ground plate. The distance between the tips of the needles and the ground plate electrode was 40–42 mm. The integrated corona charge transfer was 2.6 W. The ground plate rotated at 8 rpm in order to obtain a uniform surface exposure.

2.5. Air plasma

Specimens were subjected to air plasma in a V15-G microwave frequency reactor from Plasma-Finish GmbH, Germany. The exposures were performed at 27.0 Pa in ultra-pure air (20% O_2/80% N_2; AGA, Sweden) at a gas flow of $8.3 \times 10^{-7}\ m^3\ s^{-1}$. The frequency was 2.45 GHz and the power was 100 W.

2.6. Contact angle measurements

Dynamic contact angle measurements were made using a Ramé Hart goniometer by the sessile drop technique [25]. Deionized water (Millipore, resistivity = 18.4 MΩ cm) was used. Each data point presented in this paper is based on 10 contact angle measurements at five different positions on the specimen. Advancing and receding contact angles were measured with the needle remaining in the water droplet. The specimens were kept on glass plates (120 mm in diameter and 3 mm thick) during the corona/air plasma exposures and the subsequent contact angle measurements to avoid possible cracking of the oxidised surfaces. The temperature dependence of the hydrophobic recovery was

assessed by ageing the exposed specimens at 22 ± 2, 60 ± 2, 90 ± 2 and 114 ± 2°C. The specimens were kept in separate glass containers in the oven in order to avoid contamination.

2.7. X-ray photoelectron spectroscopy

Before the XPS analysis, the specimens were Soxhlet extracted in $CHCl_3$ for 3 h in order to remove low molar mass siloxanes formed during exposure to the corona/air plasma, and subsequently degassed in vacuum. The XPS spectra were obtained using an AXIS-HS spectrometer from Kratos Analytical. The monochromatic AlK_α radiation used was operated at 15 kV and 300 W. The pressure in the sample chamber was between 5 and 10 μPa. Survey spectra were recorded at a 80 eV pass energy and the high resolution spectra of the Si 2p peak at 20 eV pass energy. The spectra were referenced to the O1s-line (binding energy = 532.0 eV). A low-energy electron flow gun was used to neutralise sample charging. The high resolution spectra of the Si 2p peaks were resolved into three components according to Alexander et al. [26]: Si bound to two oxygen at 102.1 eV, Si bound to three oxygen at 102.8 eV and Si bound to four oxygen (SiO_2) at 103.4 eV. The peak positions were kept with an accuracy of ±0.1 eV and both the width parameters and the amplitudes of the three Gaussian peaks were adjusted in fitting the model to the experimental data. The full width at half maximum was kept below 1.5 eV. The accuracy of the fits has been estimated to be ±5% [26].

All the materials with different crosslink densities exposed to corona were analysed by XPS, whereas a number of representative specimens were analysed after exposure to air plasma. The effect of exposure time was studied for material P8. The influence of crosslink density was studied on specimens exposed to 120 s air plasma.

2.8. Optical microscopy

The fracture characteristics of the oxidised surface layers was assessed at 22 ± 2°C using a tensile testing machine mounted on a Leitz Ortholux POL BK II optical microscope. The size of the specimens were 6 ± 0.5 mm × 10 ± 0.5 mm. A small prestrain was applied to assure that the specimen was aligned properly, which induced an uncertainty of about 0.5% strain ($\varepsilon = d/l_0$, where d is the displacement and l_0 the initial length of specimen) in the measured values. The strain was increased stepwise by 2% strain increments after an initial strain step of 1%. The elongation rate was 50 ± 10 μm s^{-1} in each strain step. The time interval between the steps was 4 min. During this period, the fragmentation lengths were determined in the microscope using a micrometer scale for calibration. Each reported data point is an average value for five different locations on the specimen.

2.9. Atomic force microscopy

A Nanoscope IIIA Multimode atomic force microscope was used to assess the surface topography. The scan rate was 1.5 Hz. The surface roughness was assessed using a scanning size of 1 ± 0.2 μm × 1 ± 0.2 μm.

2.10. Scanning electron microscopy

A JEOL JSM-5400 scanning electron microscope operating at 10 kV acceleration voltage was used to assess surface cracking. The specimens were coated with Au/Pd (60/40) before examination, using a Desk II from Denton Vacuum, operating at 45 mA for 10 s. The specimens were kept in vacuum for at least 1 h before the sputtering and then immediately examined in the microscope to avoid cracking of the sputtered layer due to the release of residual dissolved gases from the bulk when the surface was hit by the electron beam in the scanning electron microscope.

3. Results

3.1. Network structure and stress–strain properties

Fig. 1 shows that the Young's modulus is proportional to the crosslink denksity ($\rho/\bar{M}_c$), as is expected from rubber elasticity theory [27]. The materials show a substantial change in Young's modulus ranging from 0.5 to 5 MPa.

The variation in density with increasing crosslink density is non-linear (Fig. 1). The densest network (P0.7) showed a significantly higher density (982.4 kg m^{-3}) than the other materials with lower crosslink density (969.5–972.2 kg m^{-3}).

3.2. Contact angle data

3.2.1. Hydrophobic recovery at 22°C

After exposure to 0.5 h corona, all the specimens exhibited

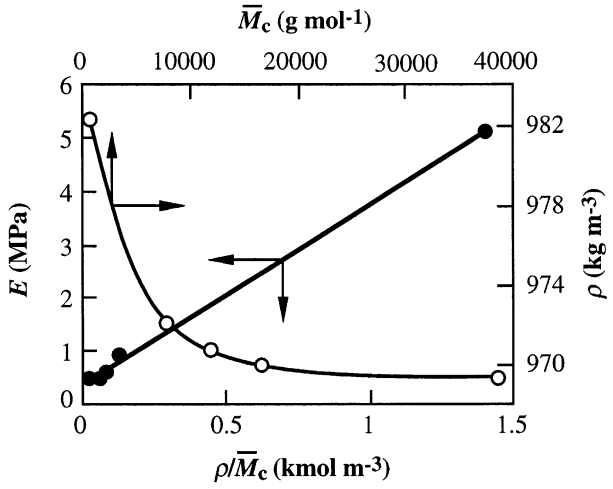

Fig. 1. Young's modulus (E) as a function of crosslink density ($\rho/\bar{M}_c$, where ρ is the density and $\bar{M}_c$ the number average molar mass of the chains between the crosslinks), and the density (ρ) as a function of $\bar{M}_c$.

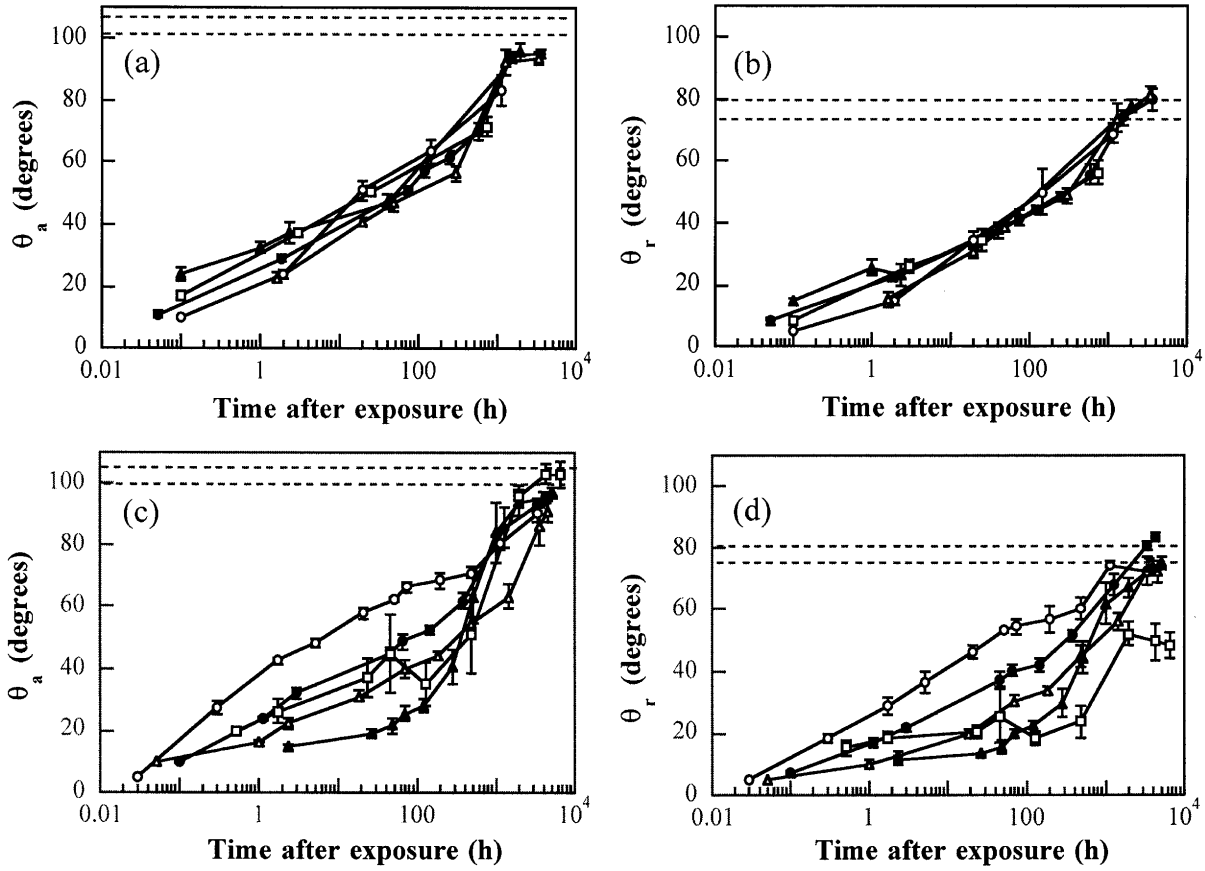

Fig. 2. Advancing (θ_a) and receding (θ_r) contact angles of PDMS networks as a function of the recovery time at 22°C after corona exposure for 0.5 h corona (a) and (b) and 1 h (c) and (d) for the following materials: P0.7 (○), P8 (●), P12 (△), P17 (▲) and P38 (□). The dotted lines indicate the range of the advancing and receding contact angles for the unexposed specimens. The error bars indicate 90% confidence intervals.

advancing (θ_a) and receding (θ_r) contact angles lower than 25° (Fig. 2a and b). The contact angles after 1 h corona were even lower, $<10°$ (Fig. 2c and d). The unexposed specimens showed contact angles between 100 and 105° (θ_a) and between 75 and 80° (θ_r). The recovery process continued over a very long period of time at 22°C, typically a few thousand hours. A general trend observed for specimens exposed to corona and plasma was that full recovery of θ_a was slower than that of θ_r (Figs. 2 and 3). This has been reported earlier by Morra et al. [8] and Hillborg and Gedde [14]. The hysteresis, i.e. the difference between advancing and receding contact angles was only 2–5° directly after the corona exposures and it increased gradually with recovery time to ~10°. The small hysteresis in freshly exposed samples is well known [14] and it reflects the low segmental mobility of the molecules in the oxidised (silica-like) top layer.

The hydrophobic recovery was insensitive to the crosslink density for the specimens exposed to 0.5 h corona (Fig. 2a and b). The variation in contact angle between the different materials was within two standard deviations. For the specimens exposed to 1 h corona, the recovery rate increased with increasing crosslink density (Fig. 2c and d). Material P38 required more than 8000 h to recover fully.

The recovery data of specimens exposed to 3 h corona resembled the rates obtained for the specimens exposed to 1 h corona. The hydrophobic recovery rates increased with increasing crosslink density. The scatter in the contact angle data was larger after the 3 h corona exposure; the initial values ranged from 2 to 19° and the recovery curves were more irregular than for the specimens exposed to 0.5 or 1 h corona.

The hydrophobic recovery of specimens exposed to air plasma showed no systematic dependence on material crosslink density (Fig. 3a–f). The contact angles were 35–45° (θ_a) and 30–35° (θ_r) immediately after 30 s air plasma exposure and less than 20° immediately after 120 and 180 s air plasma exposure. The times to reach the hydrophobicity of the unexposed materials were shorter for the specimens exposed to air plasma than for the specimens exposed to corona. The times to recover the receding contact angles decreased from 300–1000 h after 30 s air plasma to 100–500 h after 180 s air plasma. The scatter in recovery times increased progressively with increasing dose of air plasma. The hysteresis ($\theta_a - \theta_r$) was 2–5° directly after exposure to the air plasma and it increased gradually with increasing recovery time to reach a final value of 25°.

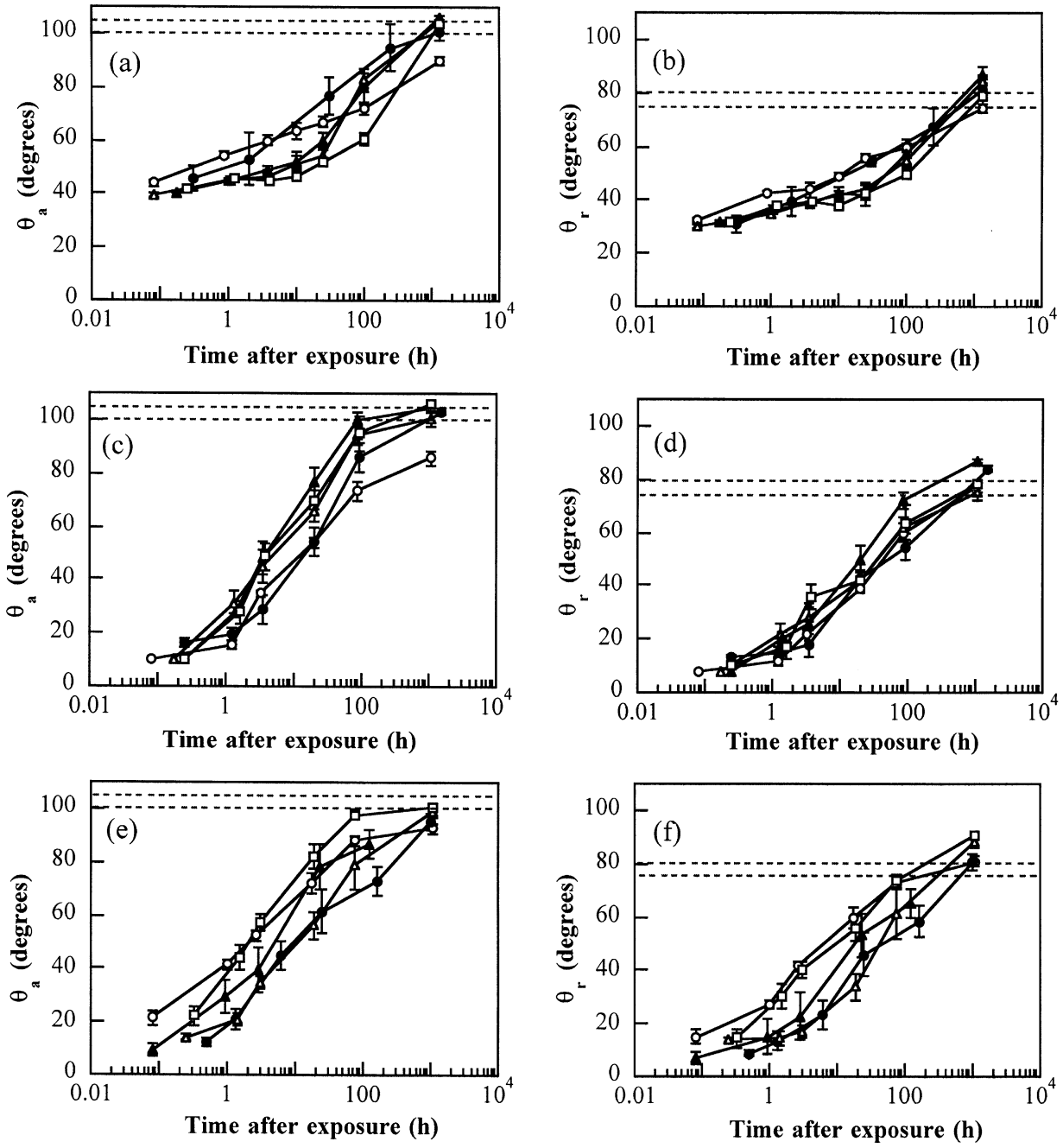

Fig. 3. Advancing (θ_a) and receding (θ_r) contact angles of PDMS networks as a function of the recovery time at 22°C after air plasma exposure for 30 s (a) and (b), 120 s (c) and (d) and 180 s (e) and (f) for the following materials: P0.7 (○), P8 (●), P12 (△), P17 (▲) and P38 (□). The error bars indicate 90% confidence intervals.

3.2.2. Temperature dependence of the hydrophobic recovery

The Arrhenius diagrams shown in Fig. 4a and b were obtained by plotting the logarithm of the reciprocal of the time to reach $\theta_r = 70°$ versus the reciprocal of the temperature. The recovery rate data for a series of materials exposed to 1 h corona are shown in Fig. 4a and they all obey the Arrhenius law. The slopes, which are proportional to the activation energies, are almost the same for the different materials; the curves being mainly only parallel shifted along the *y*-axis. The specimens that were deformed to 15% strain showed an upward jump by 1–2 orders of magnitude. The advancing contact angle data showed a similar temperature dependence but these are not shown. The hydrophobic recovery of all the specimens exposed to corona showed an Arrhenius-type temperature dependence; Table 1 presents the activation energies. The activation energy ranged between 30 and 60 kJ mol^{-1} with an average of 42 kJ mol^{-1} and a standard deviation of 10 kJ mol^{-1}. The

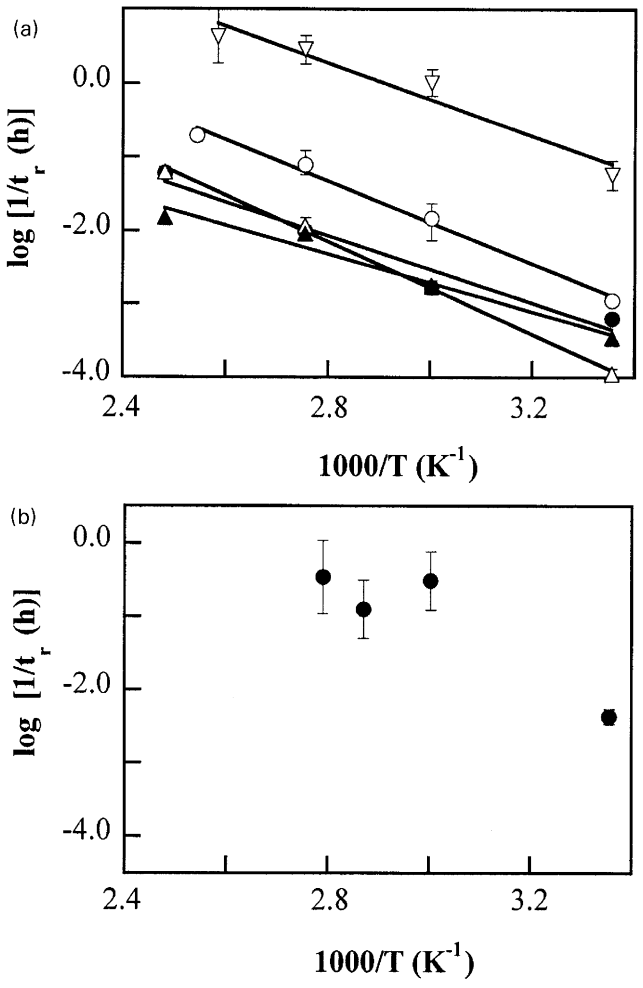

Fig. 4. (a) The logarithm of the reciprocal of the time to reach a receding contact angle of 70° after 1 h corona plotted against the reciprocal of the absolute temperature for the following materials: P0.7 (○), P7 (●), P12 (△), P17 (▲) and P12 deformed to 15% strain (▽). The error bars indicate 90% confidence intervals. (b) The logarithm of the reciprocal of the time to reach a receding contact angle of 70° plotted against the reciprocal of the absolute temperature after 120 s air plasma for P12. The error bars indicate 90% confidence intervals.

Table 1
Activation energy of hydrophobic recovery after exposure to corona (based on the recovery time to reach $\theta_r = 70°$)

Material	Corona exposure time		
	0.5 h	1 h	3 h
P0.7	53	53	30
P8	37	44 (37)[a]	53
P12	43	60 (46)[a]	31
P17	33	37 (30)[a]	53
P38	35	–[b]	–[b]

[a] Based on the recovery time to reach $\theta_r = 70°$ after applying a 15% strain; value within parentheses.
[b] Recovery to $\theta_r = 70°$ was not attained within the experimental time.

activation energy was independent of crosslink density (averages including all corona exposure times: P0.7, 43 kJ mol^{-1}; P8, 45 kJ mol^{-1}; P12, 41 kJ mol^{-1}; P17, 41 kJ mol^{-1}; P38, 35 kJ mol^{-1}) and corona exposure time (average ± standard deviation = 40 ± 8 kJ mol^{-1} (0.5 h); 49 ± 10 kJ mol^{-1} (1 h); 42 ± 13 kJ mol^{-1} (3 h)). The specimens deformed to 15% strain showed similar activation energies, average ± standard deviation = 38 ± 8 kJ mol^{-1}.

The specimens exposed to air plasma showed a very pronounced deviation from the Arrhenius law. All the data conformed to the curve form shown in Fig. 4b with a steep slope at low temperatures — the slope corresponded to an activation energy of ≈ 100–200 kJ mol^{-1} — and a flat line at the higher temperatures with a slope corresponding to a very low activation energy (<10 kJ mol^{-1}).

3.3. X-ray photoelectron spectroscopy

The elemental composition of the 8–10 nm top layer was assessed by XPS and the data are presented in Tables 2–4. The elemental composition of an unexposed PDMS was 52.2 at.% C, 23.6 at.% Si and 24.1 at.% O which is close to the theoretical elemental composition of the repeating unit of the polymer: 50 (C), 25 (Si) and 25 (O) at.%.

The carbon content decreased, whereas the oxygen content increased with increasing dose of corona/air plasma. The silicon content remained essentially constant between 24 and 28 at.%. The elemental composition is presented in Tables 2 and 4 as the ratio of the atomic concentration of carbon to that of oxygen (C/O). The unexposed materials showed C/O ratios close to 2.2. The corona exposures led to a gradual decrease in the C/O ratio with increasing exposure time (Table 2). It is also evident from the data presented in Table 3 that the C/O ratio decreased with increasing crosslink density at any given corona exposure time. Similar data were obtained for the specimens exposed to air plasma.

Further information about the structure of the top layer was obtained by resolving the Si 2p peak into three peaks according to the method developed by Alexander et al. [26]. The 102.1 eV peak is associated with Si bound to two oxygen atoms (unoxidised PDMS), the 102.8 eV peak is associated with Si bound to three oxygen atoms (partially oxidised PDMS), and the 103.4 eV peak is associated with Si bound to four oxygen atoms (SiO_2). All samples showed a

Table 2
Atomic C/O ratio of surface layer from XPS data after exposure to corona or air plasma

Material	Corona			120 s air plasma
	0.5 h	1 h	3 h	
P0.7	0.87	0.83	0.41	0.48
P8	1.20	1.08	0.79	0.82
P12	1.46	1.11	0.90	0.92
P17	1.69	1.32	1.01	1.08
P38	1.56	1.48	1.04	1.17

Table 3
Results of curve resolution of Si 2p peak for the materials studied after corona exposure

Material	Corona exposure time (h)	Intensity (%) of Si 2p peaks		
		102.1 eV	102.8 eV	103.4 eV
P0.7	0.5	36	30	34
P0.7	1	41	23	36
P0.7	3	38	18	44
P8	0.5	59	19	22
P8	1	47	31	22
P8	3	39	27	35
P12	0.5	56	32	12
P12	1	52	27	20
P12	3	49	19	32
P17	0.5	69	20	11
P17	1	69	15	16
P17	3	58	12	30
P38	0.5	73	17	11
P38	1	67	20	14
P38	3	46	25	29

similar trend in the changes in surface structure with increasing corona exposure time (Table 3), the SiO_2 content increased and the fraction of unoxidised PDMS decreased. The minimum content of unoxidised PDMS was 36 at.% and the maximum obtained SiO_2 content was 44 at.%. The content of partially oxidised PDMS (102.8 eV peak) showed in some cases a decrease with increasing corona dose (P0.7, P12 and P17), whereas in other cases, it increased (P8 and P38). The SiO_2 content increased with increasing crosslink density at any given corona dose. Material P0.7 became heavily oxidised already after 0.5 h of corona exposure. The content of unoxidised PDMS remained essentially constant on further extension of the corona exposure time. The further oxidation proceeded in this case by transformation of partially oxidised PDMS to SiO_2.

The oxidation induced by the air plasma proceeded at a much higher rate than that induced by corona. Already after 10 s air plasma exposure of P8, the C/O ratio decreased from 2.16 to 1.30 (Table 4), which was comparable to 0.5 h corona exposure (C/O ratio = 1.20). Curve resolution of the Si 2p peak showed that 25% of the PDMS had transformed into an oxidised state, consisting mainly of partially oxidised PDMS. The total amount of oxidised silicon increased with increasing exposure time, reaching a value of 60%, mainly consisting of SiO_2 (38%). This was comparable to the SiO_2 content after 3 h corona for this particular material. Longer exposures to air plasma (>180 s) led to no further change in the surface composition, which remained essentially constant at C/O $\approx 0.65 \pm 0.05$ (Table 4). The C/O ratio was also calculated from the data obtained from the curve resolution of the Si 2p peaks and these calculated values were generally lower than the values of the C/O ratios obtained from the survey spectra. The discrepancy may be explained by the fact that not all oxygen atoms are directly bonded to Si; some oxygen atoms are bonded to carbon atoms.

Table 4
Atomic C/O ratio and results of curve resolution of the Si 2p peak of the surface layer of material P8 from XPS data after exposure to air plasma

Plasma exposure time (s)	C/O	Intensity (%) of Si 2p peaks		
		102.1 eV	102.8 eV	103.4 eV
10	1.30	75	17	7
30	1.28	70	16	14
120	0.82	57	24	19
180	0.70	45	12	43
360	0.65	42	23	35
720	0.60	40	22	38

3.4. Fracture behaviour of surface layer

The mechanical properties of the silica-like layer were assessed in tensile tests, and the onset of cracking and the subsequent fragmentation process were determined as a function of strain. Specimens based on material P0.7 were not included in these studies because of their extreme brittleness even before exposure to corona or air plasma (fracture strain < 2%). The fracture patterns appeared as sharply defined cracks oriented perpendicular to the direction of the applied stress (Fig. 5). SEM and optical microscopy confirmed that these parallel cracks only appeared in strained specimens.

SEM of undeformed specimens exposed to 0.5–3 h corona revealed only a few surface cracks. Such cracks were initiated by sharp edges or at particles present on the surfaces. Specimens cut after corona/plasma exposure and subsequently sputtered, showed extensive surface cracking [22]. The overall picture is that specimens exposed to large doses of corona showed more extensive spontaneous cracking.

The surface crack pattern was characterised by the fragmentation length (L), defined as the distance between two adjacent parallel cracks. Cracks with random orientation, often initiated from defects or edges were not considered in the statistical analysis of the crack pattern. The fragmentation length data are presented in Fig. 6. Dotted lines indicate that not all the tested specimens exhibited parallel surface cracks, whereas continuous lines indicate fragmentation of all the tested specimens.

The strain for the onset of surface cracking increased with decreasing corona exposure time and decreasing crosslink density (Fig. 6a–c). Another trend in the data is the decrease in L with increasing overall strain until an almost constant value of L (4–10 μm) was established at high strains. After 0.5 h corona, only a fraction of the specimens showed fragmentation (dotted lines in Fig. 6a) and the material with the lowest crosslink density (P38) showed no fragmentation. Specimens exposed to 1 h corona showed curves that were essentially shifted along the strain axis depending on their

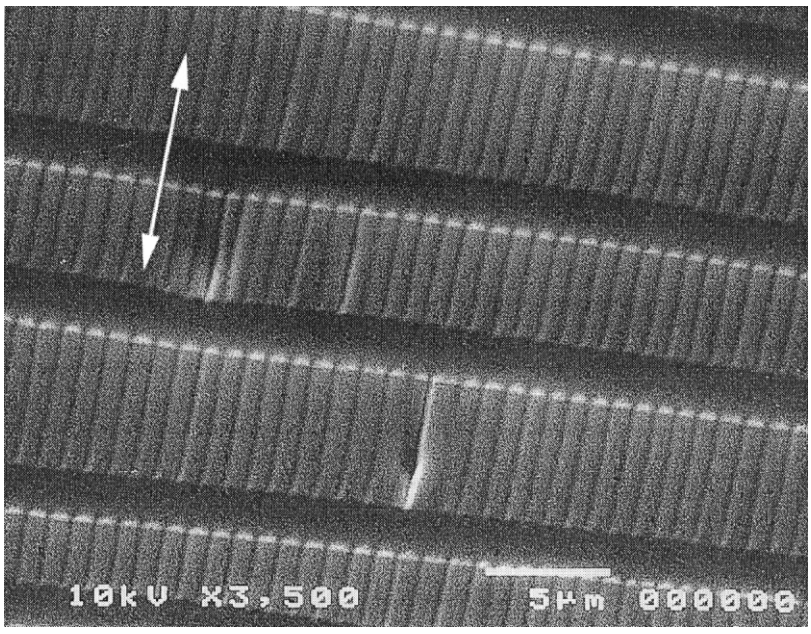

Fig. 5. Scanning electron micrograph of a strained (45% strain) P38 specimen after 180 s air plasma. The arrow indicates the direction of the applied uniaxial stress. Surface cracks are perpendicular to and buckling of the surface layer is parallel to the direction of the applied stress.

particular crosslink density, the material with the highest crosslink density being shifted to the lowest strains (Fig. 6b). Further exposure to corona (3 h) led to a fragmentation length–strain relationship almost independent of the crosslink density (Fig. 6c).

Specimens exposed to air plasma showed the same basic pattern as the specimens exposed to corona: the strain for the onset of cracking increased with decreasing dose of corona and decreasing crosslink density. The specimens exposed to 30 s air plasma showed no surface cracks, whereas some of the specimens exposed to 120 s (P17 and P38, onset of fragmentation $>10\%$) and all the specimens exposed to 180 s air plasma exhibited fragmentation. The fragmentation length showed a strain dependence similar to that of specimens exposed to corona (viz. Fig. 6a–d).

At higher strains, regular buckling of the surface parallel to the direction of stress was observed (Fig. 5). The buckling process was reversible, i.e. the buckling disappeared when the uniaxial stress was released.

3.5. Atomic force microscopy

Further details about the fragmentation pattern and surface roughness of one of the networks (P8) was obtained by AFM of specimens uniaxially deformed after exposure to corona or air plasma. After being temporarily subjected to 15 or 20% strain, the specimens were investigated using AFM. Long and almost parallel cracks oriented perpendicular to the direction of the applied stress were observed in the deformed (15% strain) specimens exposed to 1 and 3 h corona (Fig. 7a–c). Many fibrils with a diameter of approximately 10 nm bridged the crack in the specimens exposed to 1 h corona. The depth of the cracks in the deformed specimen exposed to 1 h corona was greater than 30 nm; the base of the crack was not however detectable. The cracks in the specimen exposed to 3 h corona exhibited sharper edges and only a few bridging fibrils (Fig. 7c). The crack base was detectable and hence a more exact determination of the crack depth was possible, yielding a crack depth of approximately 100 nm. The base of the crack appeared to be of the same phase as the surface, indicating that the cracks did not penetrate down to the fully unoxidised PDMS.

The transformation of the surface material from PDMS to the oxidised forms induced by the exposure to corona/air plasma leads to a substantial decrease in specific volume, which in turn introduces tensile stresses in the oxidised surface layers [22]. The stresses were relaxed by the surface cracking resulting in ‘ridges’ with an elevation of approximately 10 nm along the cracks. This characteristic feature was found in specimens exposed to corona and air plasma (Fig. 7d). The depth of the cracks formed after 120 s air plasma was greater than 10 nm, and may certainly be deeper because the base of the cracks was not detected (Fig. 7d).

The surface roughness of the regions between the parallel cracks was generally low ($R_a < 1$ nm) for all specimens. The specimen exposed to 1 h corona showed a decrease in R_a from 0.97 to 0.16 nm after deformation to 15% strain. However, the surface roughness of the uncracked regions in the specimens exposed to 3 h corona (R_a changed from 0.16 to 0.19 nm) or 120 s air plasma (R_a changed from 0.31 to 0.51 nm) remained essentially unchanged after surface cracking (15% strain).

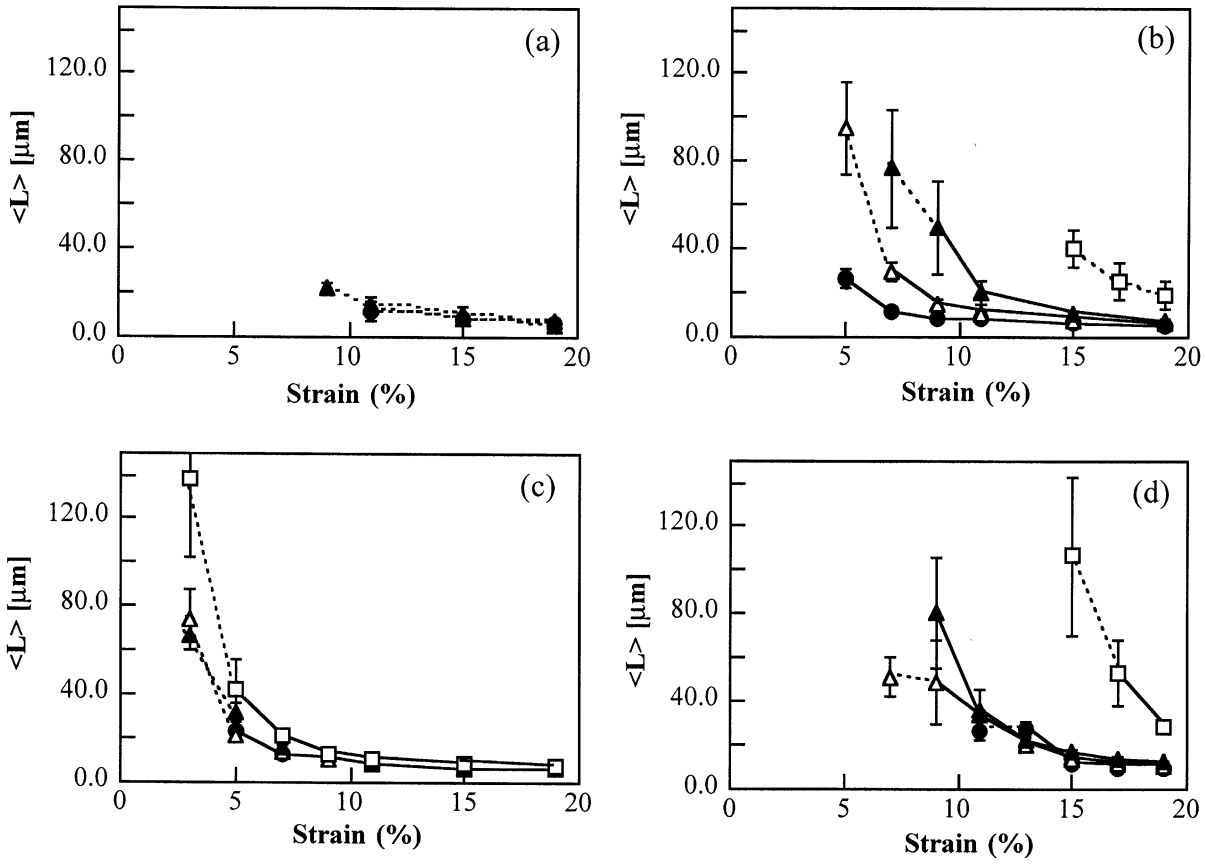

Fig. 6. Average fragmentation length (L) as a function of strain after exposure to: (a) 0.5 h corona, (b) 1 h corona; (c) 3 h corona; (d) 180 s air plasma for the following materials: P8 (●), P12 (△), P17 (▲) and P38 (□). The error bars indicate 90% confidence intervals.

4. Discussion

Fig. 8a and b shows the degree of surface oxidation by XPS expressed in the C/O ratio (Tables 2 and 4) and the percentage of unoxidised PDMS (Tables 3 and 4) as a function of dose (energy). The differences between the specimens exposed to corona and air plasma were small, typically of the order of two standard deviations of the obtained data. It seems thus that the two treatments gave roughly the same degree of surface oxidation for the same dose of exposure. Hence, no further comparisons between the methods with regard to dose will be made; the comparisons between the methods will be made on the basis of the degree of surface oxidation (C/O ratio).

XPS showed that the denser networks oxidised more rapidly in both corona and air plasma (Tables 2–4). The degree of oxidation, expressed by the C/O ratio and the degree of conversion of PDMS to the oxidised forms, increased with increasing crosslink density (Figs. 9 and 10). At low crosslink densities, the increase in oxidation degree (or rate) is almost linear with crosslink density but the rate becomes constant at higher degrees of crosslinking (Figs. 9 and 10).

The question is whether the surface structure as it is revealed in this particular analysis reflects the structure as it is directly after exposure to corona/air plasma or whether the surface layer is 'contaminated' by low molar mass PDMS species migrating from the bulk to the surface. The specimens were initially extracted to remove low molar mass species. The specimens were extracted once more and degassed in vacuum after the exposure to corona/air plasma to remove low molar mass species. Hillborg et al. [28] reported for identical PDMS materials that the main decomposition products were small cyclic siloxanes and that longer oligo(dimethyl siloxanes) were essentially absent. These volatile cyclic molecules should largely be absent from the specimen surface during the XPS analysis in view of the low pressure in the XPS chamber. It is thus believed that the structure revealed by XPS is relatively similar to the structure that exists directly after corona or air plasma exposure.

The C–C bonds are more sensitive towards oxidation than silicon with substituted methyl groups [7] and hence the denser networks with their more numerous crosslinks are more readily oxidised. The silicon atom is electron-withdrawing, resulting in polarisation of the methyl groups and rendering the latter groups less susceptible to radical attack.

A second important finding revealed by XPS is that the surface layer in all the samples, even in those extensively exposed to corona or plasma, contained a large fraction of

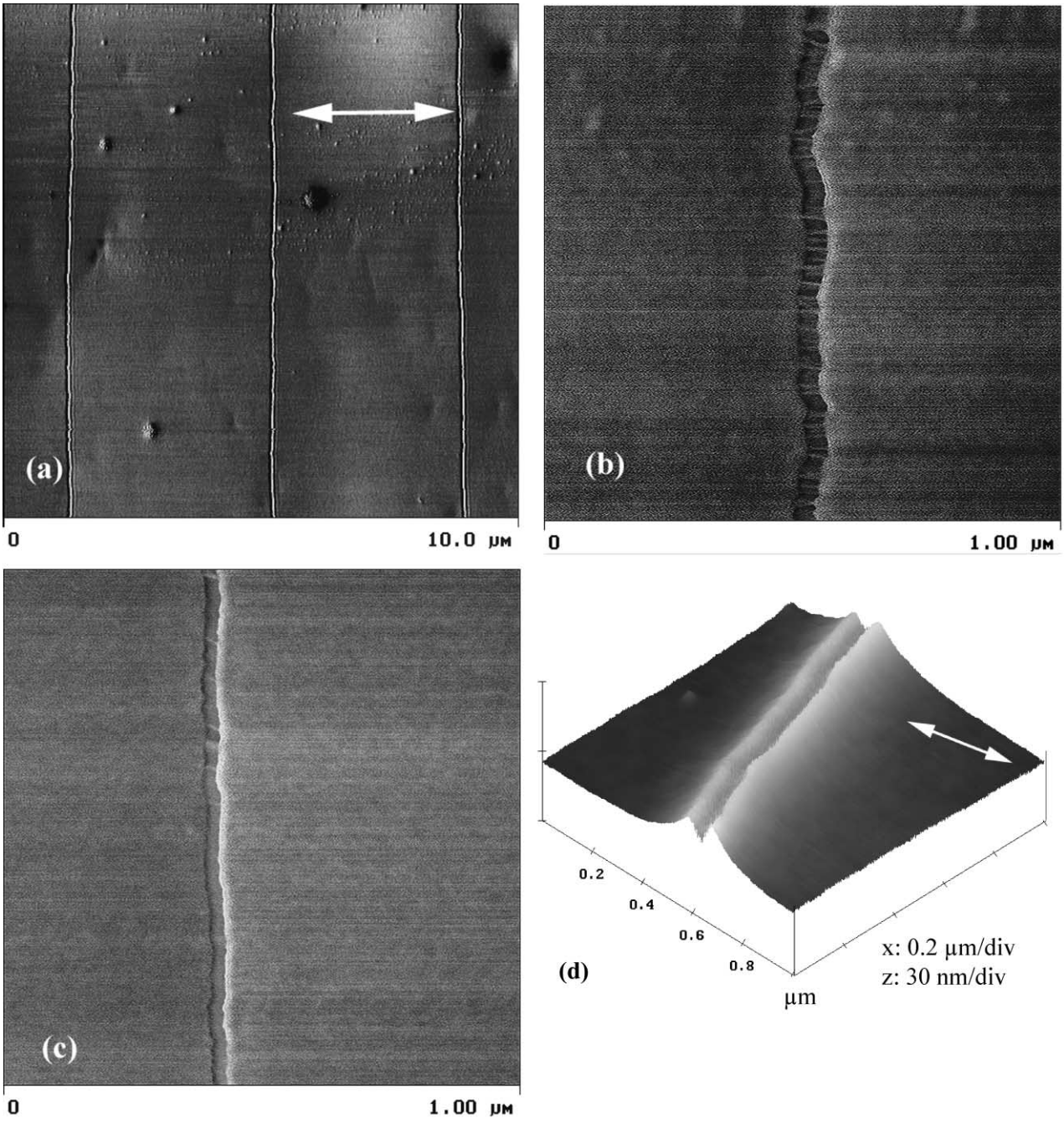

Fig. 7. Atomic force micrographs of P8 deformed after exposure to: (a) and (b) 1 h corona (15% strain); (c) 3 h corona (15% strain); (d) 120 s air plasma (20% strain). The arrow indicates the direction of the applied uniaxial stress.

unoxidised silicone, i.e. silicon bonded to only two oxygen atoms. The lowest concentration of unoxidised silicon observed was 38 at.%. It is believed that only a small part of the unoxidised silicon present in the surface layer is due to migration of low molar mass species. Hence, there must be a limiting factor of a physical and/or chemical nature that prohibits oxidation over a certain limit. One possibility is that the extensive crosslinking accompanying oxidation also reduces the segmental mobility of the unoxidised species. At some critical low value in segmental mobility, further oxidation should be impossible. Grassie and Scott [29] stated that polymers oxidise more rapidly above their glass transition temperature than in the glassy state, primarily due to the faster rate of diffusion of oxygen and to the so-called cage effect (recombination of nearby radicals). Dan and Guillet [30] showed that the quantum yield (number of molecules reacting in a particular process divided by the number of quanta absorbed by the system) for chain scission induced by UV radiation showed a pronounced jump at the glass transition temperature for a

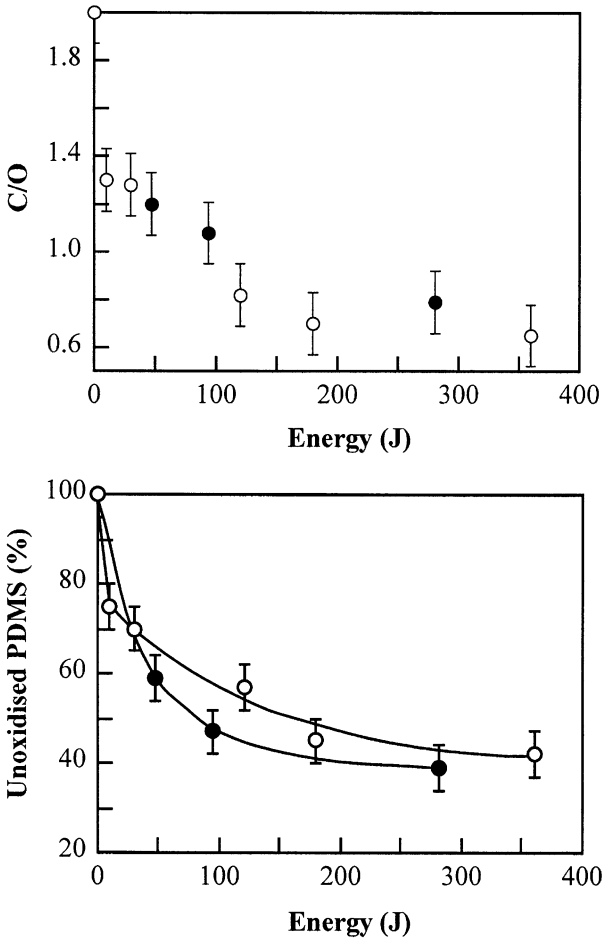

Fig. 8. (a) The carbon-to-oxygen ratio (C/O) of the surface layer determined by XPS as a function of energy (time of exposure × power) for P8: corona (●); air plasma (○). The error bars indicate the standard deviation. (b) Amount of unoxidised PDMS, based on the curve resolution of the Si 2p peak (102.1 eV) as a function of energy (time of exposure × power) for P8: corona (●), air plasma (○). The error bars indicate an estimated accuracy of 5%.

range of fully amorphous polymers. An implication is that the oxidised and unoxidised components must be mixed on a fine (submicrometer) scale. If the oxidised and unoxidised species formed separate, large domains (micrometers in size), the segmental mobility of the molecules within the unoxidised domains would be unaffected.

It is very difficult to assess the thickness of the silica-like layer. This is mostly because the oxidised layer may consist of several sub-layers or even of material exhibiting a smooth change in the degree of oxidation. Neutron reflectometry showed that the thickness of the oxidised layer in PDMS exposed to oxygen plasma was of the order of 130–160 nm and that the thickness did not increase with increasing plasma dose [22]. In the few cases where the base of the crack was readily visible by AFM (3 h corona, Fig. 7c), the crack depth was of the order of 100 nm. It is clearly possible that the cracks penetrate into the unoxidised bulk material. However, AFM showed that the base of the crack was the

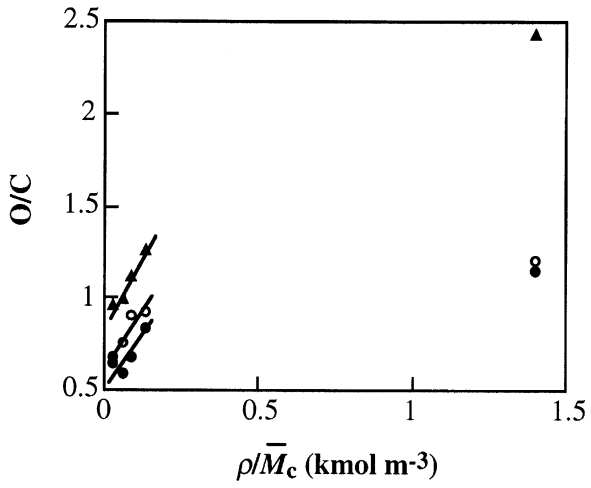

Fig. 9. The carbon-to-oxygen ratio (C/O) of the surface layer determined by XPS as a function of the crosslink density ($\rho/\bar{M}_c$, where ρ is the density and $\bar{M}_c$ the number average molar mass of the chains between the crosslinks) for specimens exposed to corona for 0.5 h (●), 1 h (○) and 3 h (▲).

same phase as the surface. In most cases, the base of the crack was not detected and a lower limit for the crack depth could only be determined. The depth of the cracks in specimens exposed to air plasma seemed to be smaller (120 s: >10 nm) than in specimens exposed to corona (1 h: >30 nm; 3 h: ~100 nm). These findings can be generalised into a scheme. The depth of oxidation is of the order of 100–150 nm and it remains constant even after prolonged exposure. The silica-like layer is thus a sub-layer of the oxidised layer. At some critical level of crosslinking (degree of conversion to the oxidised forms), vitrification occurs. The silica-like layer thus grows in thickness with increasing corona exposure but never beyond the thickness of the oxidised layer.

No absolute proof of microporosity in the silica-like layer

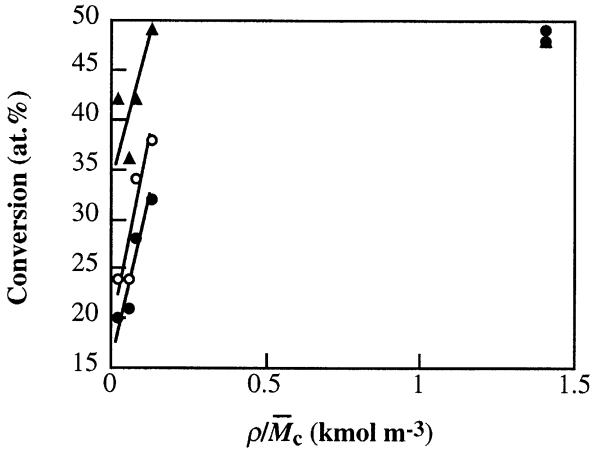

Fig. 10. Degree of conversion of PDMS to oxidised forms — silicon bonded to three oxygen atoms (weight factor = 0.5) and silicon bonded to four oxygen atoms, SiO_2 (weight factor = 1) — of the surface layer by XPS as a function of the crosslink density ($\rho/\bar{M}_c$, where ρ is the density and $\bar{M}_c$ the number average molar mass of the chains between the crosslinks) for specimens exposed to corona for 0.5 h (●), 1 h (○) and 3 h (▲).

was obtained by AFM. However, in one case, P8 exposed to 1 h corona, the surface roughness (a possible sign of micropores) of the regions between the cracks decreased when the surface layer cracked. The release of the tensile stresses in the surface possibly led to the closing of pores. Specimens subjected to longer exposures to corona or air plasma showed, however, no such jump in the surface roughness accompanying surface cracking. It is possible that these more highly oxidised surfaces possessed a more rigid pore structure.

Fig. 11 shows a summary of the fracture strain of the different oxidised layers. The fracture strain increases, as expected, with increasing C/O ratio. At the same degree of oxidation (C/O), the strain for the onset of fragmentation decreased with decreasing crosslink density. This was probably due to the increased difference in modulus between the surface layer and the bulk. Surface cracking occurred at much lower strains in the specimens exposed to corona than in those exposed to air plasma and oxidised to the same degree according to XPS. This difference in fracture behaviour possibly reflects a thinner silica-like layer in the air-plasma-exposed specimens [31]. The atomic force micrographs also showed a substantial difference in the fracture pattern; the specimens exposed to corona showed cracks with a more brittle character with sharper edges and fewer bridging fibrils than the specimens exposed to air plasma (Fig. 7).

The ductile behaviour of the surface layers evident in the tensile testing (Fig. 6a), in combination with the XPS data (Tables 2 and 3) showing a relatively low content of the oxidation products, suggests that the silica-like layer was not fully developed in P8, P12, P17 or P38 after 0.5 h corona. The hydrophobic recovery curves (Fig. 2a and b) were essentially the same for all the materials, suggesting that the same mechanism, diffusion of the oligomers through the uncracked oxidised layer, prevailed in all the materials. Corona exposure for 1 h led to the formation of a

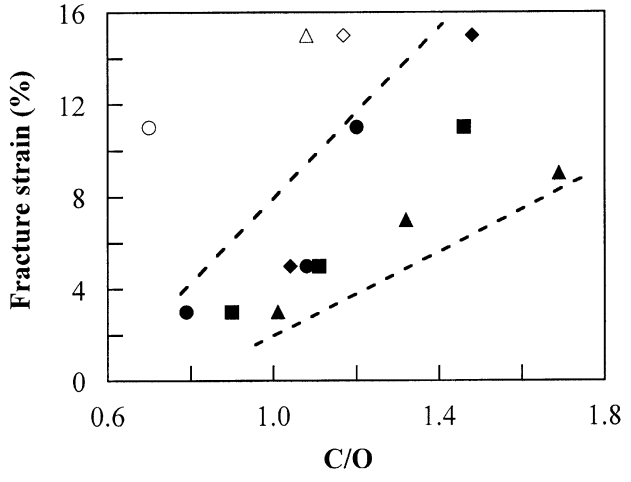

Fig. 11. Fracture strain of the oxidised layers as a function of the carbon-to-oxygen (C/O) ratio after exposure to corona: P8 (●); P12 (■); P17 (▲); P38 (◆) or air plasma: P8 (○); P17 (△); P38 (◇). The dotted lines are added as visual guides.

vitrified silica-like layer, particularly in the materials with the denser networks (note that the degree of surface oxidation increased with decreasing $\bar{M}_c$ — Tables 2 and 3). The strain for the onset of fragmentation increased with increasing $\bar{M}_c$ (Fig. 6b). Hence, the materials with the densest networks were more oxidised and they had more developed silica-like layers that cracked more readily. The hydrophobic recovery curves differed depending on the crosslink density; materials with the lowest $\bar{M}_c$ showing the fastest recovery (Fig. 2b and c). It is suggested that the faster hydrophobic recovery in the materials with the denser networks was due to the transport of oligomers through cracks/pores in the vitrified surface layer. These specimens were not cracked by an applied stress (deformation). Instead, they showed self-cracking, and this tendency was more evident in the materials with lower $\bar{M}_c$ that oxidised more readily. The strong accelerating effect of cracking was demonstrated by stretching a specimen to 15% strain, which led to an increase in the recovery rate by 1–2 orders of magnitude (Fig. 4a). Longer corona exposure (3 h) led to further oxidation and an even more brittle silica-like layer (fragmentation occurred at ~3% strain) that also exhibited self-cracking. The trend in the hydrophobic recovery data was very similar to that after 1 h corona.

The hydrophobic recovery of the specimens exposed to air plasma was essentially independent of the crosslink density (Fig. 3a–f), which was very different from the behaviour of the specimens exposed to corona (Fig. 2a–d). The oxidation rate as revealed by XPS increased in the cases of both air plasma and corona with decreasing $\bar{M}_c$ (Table 3). The fragmentation length data shown in Fig. 6d were similar for the different materials except for P38, which required a larger strain to crack. More important is the fact that the lowest strain required to cause fragmentation was >10% in the case of 120 s air plasma, which was considerably higher than the ~5% which was sufficient for the specimens exposed to 1 and 3 h corona. Thus, the silica-like layer in the specimens exposed to air plasma showed a higher fracture toughness than that in the specimens exposed to corona which showed the same degree of surface oxidation according to XPS. This difference in fracture toughness can be traced back to AFM data which showed that the vitrified layer was thinner in the air-plasma-exposed specimens than in corona-exposed specimens with the same degree of surface oxidation as revealed by XPS. It is thus suggested that self-cracking was a rare event in the specimens exposed to air plasma for 30, 120 and 180 s and that the small differences in hydrophobic recovery rate were due to the differences in degree of oxidation of the uncracked silica-like layer.

The activation energies for hydrophobic recovery after exposure to corona were very similar to those reported previously, 35–54 kJ mol^{-1} [14,32]. The activation energies obtained were independent of the crosslink density and of the corona exposure time (Table 1). It thus seem that the activation energies are the same for recovery by migration

of oligomers through the 'mildly' oxidised layer (corona exposure time = 0.5 h) and for recovery by transport of oligomers through cracks/pores in the silica-like layer (corona exposure time = 1 and 3 h). The diffusing low molar mass siloxanes which restore hydrophobicity consists mainly of cyclic oligomers, ranging from 4 to 10 repeating units [28]. The activation energies for diffusion of such species in unoxidised silicone rubber has been determined from sorption data [33]: 6–7 kJ mol^{-1} for D_4 and D_5; 16 kJ mol^{-1} for PDMS with $\bar{M}_n$ between 1000 and 40 000 g mol^{-1}. The higher activation energies obtained for the hydrophobic recovery show that the denser oxidised surface layer thus retards the transport of the oligomers. In the case of a mild oxidation, when a vitrified layer is absent, the recovery process also may involve reorientation of the polar groups by conformational changes.

The specimens exposed to air plasma showed a pronounced curvature in the Arrhenius diagram; a good example is shown in Fig. 4b. It is proposed that the non-Arrhenius behaviour is a characteristic feature of specimens with a silica-like layer with little spontaneous cracking. The following scheme provides a qualitative explanation of the non-Arrhenius behaviour. The glassy, crack-free layer acts an effective barrier for transport of oligomers at 22°C. Long recovery times are then observed. If the glass transition of this layer is between 22 and 60°C, the transformation from a glassy to a rubbery state will increase the oligomer diffusion rate significantly. Fast recovery rates are then observed. This transition will also occur in cracked surfaces, but the impact on the hydrophobic recovery rate will be less significant due to the previous transport through the cracks to the surface. The lower apparent activation energy of the recovery at the higher temperatures is consistent with the transport of oligomers through a semi-rubbery state.

5. Conclusions

PDMSs with different crosslink densities were exposed to corona discharges or GHz air plasma. XPS showed that surface oxidation was faster in more highly crosslinked polymers. This finding can be explained by the higher susceptibility to oxidation of the C–C bonds in the crosslinks than of the repeating unit of the polymer. Microscopy confirmed the presence of a brittle, microporous silica-like layer within the oxidised layer, with a minimum organic silicone content of 40% according to XPS. An implication of this finding is that the oxidised and unoxidised components must be mixed on a fine (submicrometer) scale. The unoxidised regions are shielded from further oxidation by the surrounding oxidised (vitrified) phase, which acts as a cage for active radicals. The thickness of the silica-like layer increased with increasing corona exposure time reaching a thickness of approximately 100 nm after 3 h corona, which is of the same order of magnitude as the thickness of the oxidised layer. Specimens exposed to air plasma developed thinner silica-like layers than those exposed to corona with the same degree of surface oxidation. The strain at which the silica-like layer cracked decreased with increasing corona/air plasma exposure time. The hydrophobic recovery following the corona/air plasma exposure occurred at a slow rate by diffusion of oligomers through the microporous but uncracked silica-like layer or at a much higher rate by transport of oligomers through cracks in the silica-like layer. The hydrophobic recovery of specimens exposed to corona exhibited an Arrhenius-temperature-dependence with activation energies near 40 kJ mol^{-1} both for mildly oxidised specimens without a glassy silica-like layer and for specimens with a cracked silica-like layer. The hydrophobic recovery of the specimens exposed to air plasma showed a pronounced curvature in the Arrhenius diagram. It is suggested that this behaviour is characteristic of specimens with thin, uncracked silica-like layers; the steep slope in the Arrhenius diagram at low temperatures reflects the glassy state and the flatter part at high temperatures a more rubber-like state.

Acknowledgements

The Swedish Research Council for Engineering Sciences (TFR: grant 285-95-606) and ABB Corporate Research, Västerås are thanked for this sponsorship. B. Olander, Department of Polymer Technology, Royal Institute of Technology is thanked for carrying out the XPS measurements.

References

[1] Kindersberger J, Schütz A, Kärner HC, Huir R. CIGRE 1996:33–303.
[2] Kunde K, Hennings R, Kuhl M, Schütz A, Janssen H, Stietzel U. CIGRE 1998:15–206.
[3] Vlastós AE, Gubanski SM. IEEE Trans Power Deliv 1991;6:888.
[4] Sörqvist T, Karlsson U, Vlastós AE. In: Proceedings of the Ninth International Symposium on High Voltage Engineering, 1995. p. 3234.
[5] Gubanski SM, Vlastós AE. IEEE Trans Power Deliv 1990;5:1527.
[6] Kim SH, Cherney EA, Hackam R. IEEE Trans Power Deliv 1991;6:1549.
[7] Owen MJ. In: Ziegler JM, Fearon FWG, editors. Silicon-based polymer science, a comprehensive resource, Adv Chem Ser 224. Washington, DC: American Chemical Society, 1990.
[8] Morra M, Occhiello E, Marola R, Garbassi F, Humphrey P, Johnson D. J Colloid Interf Sci 1990;137:11.
[9] Tóth A, Bertóti I, Blazsó M, Bánhegyi G, Bognar A, Szaplonczay X. J Appl Polym Sci 1994;52:1293.
[10] Lee CL, Homan GR. IEEE Int Conf Electr Phen Electr Insul 1981:435.
[11] Kim SH, Cherney EA, Hackam R, Rutherford KG. IEEE Trans Dielectr Electr Insul 1994;1:106.
[12] Owen MJ, Smith PJ. J Adhes Sci Technol 1994;10:1063.
[13] Fritz JL, Owen MJ. J Adhes 1995;54:33.
[14] Hillborg H, Gedde UW. Polymer 1998;39:1991.
[15] Thomas TH, Kendrick TC. J Polym Sci, Part A-2 1969;7:537.
[16] Lee LH. J Adhes 1972;4:39.
[17] Blazsó M, Garzó G, Székely T. Chromatographia 1972;5:485.
[18] Grassie N, Macfarlane IG. Eur Polym J 1978;14:875.

[19] Nielsen JM. J Appl Polym Sci, Appl Polym Symp 1979;35:223.
[20] Smith PJ, Owen MJ, Holm PH, Toskey GA. IEEE Int Conf Electr Phen Electr Insul 1992:829.
[21] Hillborg H, Gedde UW. IEEE Int Conf Electr Phen Electr Insul 1999:751.
[22] Hillborg H, Ankner JF, Gedde UW, Smith GD, Yasuda HK, Wikström K. Polymer 2000;41:6851.
[23] Chua DBH, Ng HT, Li SFY. Appl Phys Lett 2000;76:721.
[24] Wroble D. In: Auner N, Weis J, editors. Organosilicon chemistry II. Weinheim: VCH, 1996.
[25] Garbassi F, Morra M, Occhiello E. Polymer surfaces: from physics to technology. Chichester: Wiley, 1998.
[26] Alexander MR, Short RD, Jones FR, Michaeli W, Blomfield CJ. Appl Surf Sci 1999;137:179.
[27] Treloar LRG. The physics of rubber elasticity. 3rd ed. Oxford: Clarendon Press, 1975.
[28] Hillborg H, Karlsson S, Gedde UW. Polymer, submitted for publication.
[29] Grassie N, Scott G. Polymer degradation and stabilisation. Cambridge: Cambridge University Press, 1985.
[30] Dan E, Guillet JE. Macromolecules 1973;6:230.
[31] Leterrier Y, Anderson J, Pitton Y, Månson JAE. J Polym Sci, Polym Phys Ed 1997;35:1463.
[32] Kim J, Chaudhury MK, Owen MJ. IEEE Trans Dielectr Electr Insul 1999;6:695.
[33] Gedde UW, Hellebuych A, Hedenqvist M. Polym Engng Sci 1996;36:2077.